Hierarchical Visual Primitive Experts for Compositional Zero-Shot Learning

Hanjae Kim[1]   Jiyoung Lee[2]   Seongheon Park[1]   Kwanghoon Sohn[1,3,*]

[1]Yonsei University   [2]NAVER AI Lab   [3]Korea Institute of Science and Technology (KIST)

{incohjk,sam121796,khsohn}@yonsei.ac.kr   lee.j@navercorp.com

Abstract

Compositional zero-shot learning (CZSL) aims to recognize unseen compositions with prior knowledge of known primitives (attribute and object). Previous works for CZSL often suffer from grasping the contextuality between attribute and object, as well as the discriminability of visual features, and the long-tailed distribution of real-world compositional data. We propose a simple and scalable framework called Composition Transformer (CoT) to address these issues. CoT employs object and attribute experts in distinctive manners to generate representative embeddings, using the visual network hierarchically. The object expert extracts representative object embeddings from the final layer in a bottom-up manner, while the attribute expert makes attribute embeddings in a top-down manner with a proposed object-guided attention module that models contextuality explicitly. To remedy biased prediction caused by imbalanced data distribution, we develop a simple minority attribute augmentation (MAA) that synthesizes virtual samples by mixing two images and oversampling minority attribute classes. Our method achieves SoTA performance on several benchmarks, including MIT-States, C-GQA, and VAW-CZSL. We also demonstrate the effectiveness of CoT in improving visual discrimination and addressing the model bias from the imbalanced data distribution. The code is available at https://github.com/HanjaeKim98/CoT.

1. Introduction

Humans perceive entities as hierarchies of parts; for example, we recognize 'Cute Cat' by composing the meaning of 'Cute' and 'Cat'. People can even perceive new concepts by composing the primitive meanings they already knew. Such compositionality is a fundamental ability of hu-
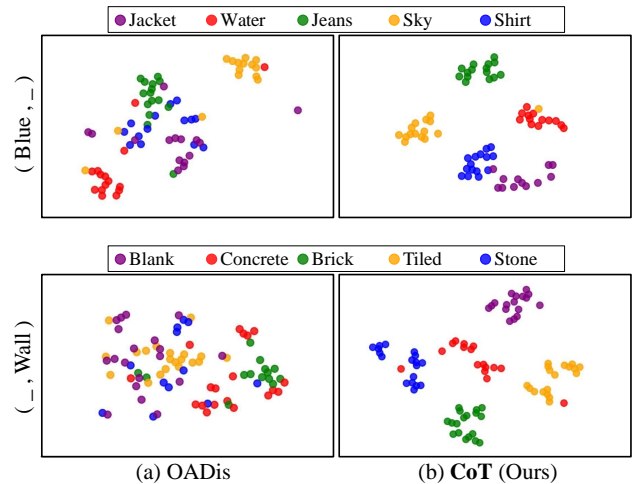

Figure 1: Visual feature distribution of previous state-of-the-art approach (OADis) [54] and **CoT** (Ours). The features are gathered with respect to attribute 'Blue -' (Top) and object '- Wall' (Bottom). Notably, the previous method suffers from degraded visual discrimination such as ('Blue, Jeans' *vs.* 'Blue, Shirt'), or all attributes composed into object 'Wall'.

mans for all cognition. For this reason, compositional zero-shot learning (CZSL), recognizing a novel composition of known components (*i.e.*, object and attribute), has been regarded as a crucial problem in the research community.

A naive approach for CZSL is to combine attribute and object scores estimated from individually trained classifiers [40, 22]. However, it is hard for these independent predictions to consider the interactions that result from a combination of different primitives, which is *contextuality* (*e.g.* different meaning of 'Old' in 'Old Car' and 'Old Cat') in the composition [40]. Previous approaches [43, 77, 37, 42, 54, 81] have solved the problem by modeling the compositional label (text) embedding for each class. They leverage external knowledge bases like Glove [38, 48] to extract attribute and object semantic vectors, and concatenate them with a few layers into the composition label embedding. The embeddings are then aligned with visual features in the shared embedding space, where the recognition of unseen image

query becomes the nearest neighbor search problem [37]. Nevertheless, the extent to which contextuality is taken into account in the visual domain has still been restricted.

Prior works [53, 54] have also pointed out the importance of *discriminability* in visual features, which is related to generalization performance towards unseen composition recognition [63, 39]. A popular solution is disentanglement [53, 54, 28, 81], in which independent layers are allocated to extract intermediate visual representations of attribute and object. However, as shown in Fig. 1, it may be challenging to extract their unique characteristics to understand the heterogeneous interaction. We carefully argue that this problem arises from how the visual backbone (*e.g.* ResNet18 [17]) is used. This is because attribute and object features, which require completely different characteristics [31, 23], are based on the same visual representation from the deep layer of the backbone.

Another challenge in CZSL is the long-tailed distribution of real-world compositional data [2, 64, 3]. Few attribute classes are dominantly associated with objects, which may cause a hubness problem [10, 12] among visual features. The visual features from the head (frequent) composition become a hub, which aggravates the visual features to be indistinguishable in the embedding space [12], and induces a *biased prediction* towards dominant composition [62, 82].

In this paper, based on the discussions above, we propose Composition Transformer (CoT) to enlarge the visual discrimination for robust CZSL. Motivated by bottom-up and top-down attention [32, 33, 29], the CoT presents object and attribute experts, each forming its feature in different layers of the visual network. Specifically, the object expert generates a representative object embedding from the last layer (*i.e.*, bottom-up pathway) that is most robust to identify object category with high-level semantics [73, 45]. Then we explicitly model contextuality through an object-guided attention module that explores intermediate layers of the backbone network and builds attribute-related features associated with the object (*i.e.*, top-down pathway). Based on this module, the attribute expert generates a distinctive attribute embedding in conjunction with the object embedding. By utilizing all the features of each layer exhibiting different characteristics, our method comprehensively leverages a visual network to diversify the components' features in the shared embedding space.

Finally, we further develop a simple minority attribute augmentation (MAA) methodology tailored for CZSL to address the biased prediction caused by imbalanced data distribution [62]. Unlike GAN-based augmentations [57, 28] that lead to overwhelming computation during training, our method simplifies the synthesis process of the virtual sample by blending two images while oversampling minority attribute classes [7, 46]. Thanks to the label smoothing effect of the balanced data distribution by augmenta-

tion [80, 60], the CoT is well generalized with minimal computational costs, resolving the bias problem induced by the majority classes.

Our contributions are summarized in three-folds:

- To enhance visual discrimination and contextuality, we propose a Composition Transformer (CoT). In this framework, object and attribute experts hierarchically estimate primitive embeddings by fully utilizing intermediate outputs of the visual network.

- We introduce a simple yet robust MAA that alleviates dominant prediction on head compositions with majority attributes.

- The remarkable experimental results demonstrate that our CoT and MAA are harmonized to improve the performance on several CZSL benchmarks, showing state-of-the-art performance.

2. Related Work

Given a set of objects and their associated attributes, compositional zero-shot learning (CZSL) aims to recognize unseen compositions using primitive knowledge. Contrary to conventional methods [35] that recognize the object and attribute independently, recent approaches [40, 43, 30] have regarded contextuality as a crucial standpoint for understanding the interpretation of the attribute depending on the object class. For example, AttrOps [43] represented the attribute as a linear transformation of the object's state, and SymNets [30] regularized visual features to satisfy the group axioms with auxiliary losses. Some works [42, 76] have leveraged graph networks to model the global dependencies among primitives and their compositions.

However, those methods have often suffered in distinguishing visual composition features. Meta-learning [13] has been utilized for CZSL frameworks [50, 68] to enhance the discriminative power of visual features but induce high training costs. Other works [53, 28, 54] have disentangled representations of objects and attributes for modeling visual composition. Those methods have shown promising generalization performance than conventional methods. However, the aforementioned approaches have often failed to discriminate the minority classes in object and attribute, which is caused by severe model bias toward seen compositions [62, 82]. They have used the mostly-shared visual backbone for attribute and object representations, which needs more deep concern to be extracted differently according to its characteristics. In specific, the attribute feature is changed in a wide variety of aspects as the property of the object changes, and the object feature must be perceived as semantically the same despite changing the attribute.

Our method is also closely related to visual attribute prediction [47, 27], where the goal is to recognize visual attributes describing states or properties within an object.
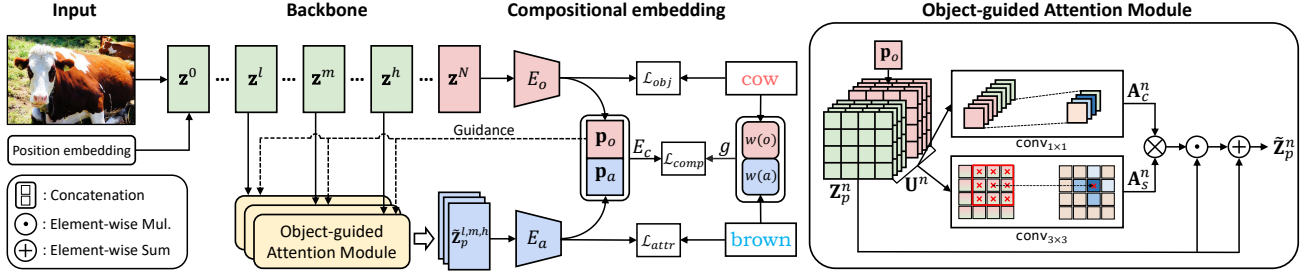
Figure 2: The overall architecture of composition transformer. Object and attribute experts produce object- and attribute-specific features at different layers. An object-guided attention module is attached to each attribute experts to highlight attribute-specific features. Object-attribute embeddings are composed, and then projected to a joint embedding space with label embedding for optimization.

Since the fine-grained local information (*e.g.* color, shape, and style) is required to the task, several approaches [56, 61, 21, 59, 49] utilize low-level features in backbone network, which contain textual details and objects' contour information [75, 70]. Meanwhile, with a similar motivation, some methods for CZSL have integrated low-level features with a multi-scale fusion approach to acquire robust visual features [71, 76]. Although a simple integrated feature can recover spatial details slightly, it is hard to localize the RoI of the attribute that varies with the object for compositional recognition; for example, a puddle in an object 'Street' for a composition class 'Wet Street'.

Moreover, attributes in generic objects are long-tailed distributed in nature [56, 49]. The imbalance issue occurs as a biased recognition problem, because deep networks tend to be over-confident in head composition classes [55, 66]. This phenomenon is also known as a hubness problem [10, 12], where few visual features from head composition classes become indistinguishable from many tail composition samples. One major solution for the data imbalance problem is the resampling [16, 58, 14, 36] by flattening the long-tailed dataset by over-sampling of minority classes or under-sampling of majority classes. However, directly applying such sampling strategies in CZSL could intensify the overfitting problem on over-sampled classes, and discard valuable samples for learning the alignment between visual and semantic (linguistic) features in the joint embedding space [82]. Another line of work is generation methods [69, 67] that hallucinate a new sample from rare classes but they require complicated training strategies for data generation. In this work, we are inspired by recent data augmentation techniques [78, 7, 46, 80, 8], and combine both resampling and generation approaches to tailor for CZSL, which facilitates the regularization of robust embedding space even in the minority classes via augmented virtual samples.

3. Composition Transformer (CoT)

In compositional zero-shot learning (CZSL), given an object set $\mathcal{O}$ and an attribute set $\mathcal{A}$, object-attribute pairs comprise a composition set $\mathcal{Y}=\mathcal{A}\times\mathcal{O}$. The network is trained with an observable (seen) composition set $\mathcal{D}_{\text{tr}}=\{\mathcal{X}_{\text{s}}, \mathcal{Y}_{\text{s}}\}$, where $\mathcal{X}_{\text{s}}$ is an image set corresponding to a composition label set $\mathcal{Y}_{\text{s}}$. Following the generalized zero-shot setting [50, 5, 74], a test set $\mathcal{D}_{\text{te}}=\{\mathcal{X}_{\text{te}}, \mathcal{Y}_{\text{te}}\}$ consists of samples drawn from both seen and unseen composition classes, *i.e.* $\mathcal{Y}_{\text{te}}=\mathcal{Y}_{\text{s}}\cup\mathcal{Y}_{\text{u}}$ and $\mathcal{Y}_{\text{s}}\cap\mathcal{Y}_{\text{u}}=\varnothing$. For this task, a powerful visual network is required to extract distinct features of objects and attributes respectively, in order to recognize both seen and unseen compositions well.

To this end, we propose a novel composition transformer (CoT) that includes object and attribute expert modules as illustrated in Fig. 2. Our CoT is basically built on the vision transformer (*i.e.* ViT [11]) and fully utilizes intermediate blocks to capture the attribute and object representations. These representations are projected into the joint embedding space to calculate the similarity between given compositional labels and images. We also introduce a minority attribute sampling method for data augmentation such that the biased recognition with head composition class is alleviated by label-smoothing regularization effect [41]. Next, we describe in detail the configurations of CoT.

3.1. Object expert

The CoT is composed of a sequence of transformer blocks including multi-head self-attention and MLP layers. Generally, as the block becomes deeper, class discrimination capability is increased while being invariant from the attribute deformation [79, 44]. Therefore, we select the final output from the last block to an input of the object expert in a bottom-up manner [32, 1].

Formally, let us denote $\{\mathbf{z}^n\}_{n=1}^N$ as the output features of the blocks in CoT. The feature of n-th transformer blocks, $\mathbf{z}^n$, consists of a class token (*i.e.*, [CLS]) $\mathbf{z}_c^n \in \mathbb{R}^{1\times D}$ and a set of patch tokens $\mathbf{z}_p^n \in \mathbb{R}^{HW\times D}$. The object expert E_o encodes the last feature to present an object embedding:

$$\mathbf{p}_o = E_o(\mathbf{z}_c^N), \qquad (1)$$

where E_o consists of a fully-connected (FC) layer. To optimize the parameters in the object expert, we compute a

cross-entropy loss with an object classifier whose weights are initialized from object word-embeddings as follows:

$$\mathcal{L}_{\text{obj}} = -\log \frac{\exp\{cos(\mathbf{p}_o, w(o_i))/\tau_o\}}{\sum_{o_k \in \mathcal{O}} \exp\{cos(\mathbf{p}_o, w(o_k))/\tau_o\}}, \quad (2)$$

where τ is a temperature parameter, $w(o)$ denotes the word-embedding [48] corresponding to the object $o \in \mathcal{O}$.

3.2. Attribute expert

Capturing both attribute and object in the same deeply condensed feature is nontrivial as they require pretty different visual representations [31, 23]. The straightforward solution is to design two-stream networks without any parameter sharing. However, such individual training could not capture the contextuality [40]. Hence, we build an attribute expert which utilizes semantics estimated from the object expert as a condition, and extracts attribute-related features on intermediate layers of visual backbone in a top-down fashion [32, 1]. We devise an object-guided attention module that leverages convolution kernel-based attention [72, 6, 25], which excels at capturing fine-grained local information required for attribute recognition [19].

Specifically, we first reshape $\mathbf{z}_p^n$ to $\mathbf{Z}_p^n$ with output resolution of $H \times W \times D$. Following [52], we tile $\mathbf{p}_o$ to match the spatial dimension with $\mathbf{Z}_p^n$ and concatenate them to obtain an object-contextualized feature $\{\mathbf{U}^n = [\mathbf{p}_o, \mathbf{Z}_p^n]\} \in \mathbb{R}^{H \times W \times 2D}$. As shown in Fig. 2, we generate a channel attention map $\mathbf{A}_c^n \in \mathbb{R}^{1 \times 1 \times D}$ from the averaged feature across the *spatial* axis:

$$\mathbf{A}_c^n = \sigma(\texttt{conv}_{1\times1}(\texttt{avgpool}_{\text{spatial}}(\mathbf{U}^n))), \quad (3)$$

where σ denotes a sigmoid function. We also generate a spatial attention map $\mathbf{A}_s^n \in \mathbb{R}^{H \times W \times 1}$ from the averaged feature across the *channel* axis:

$$\mathbf{A}_s^n = \sigma(\texttt{conv}_{3\times3}(\texttt{avgpool}_{\text{channel}}(\mathbf{U}^n))). \quad (4)$$

Finally, we aggregate two attention maps into a unified attention map $\mathbf{A}^n \in \mathbb{R}^{H \times W \times D}$ as follows:

$$\mathbf{A}^n = \mathbf{A}_s^n \times \mathbf{A}_c^n. \quad (5)$$

The output of our object-guided attention module is defined as attribute features with estimated attention maps, followed by the residual connection:

$$\tilde{\mathbf{Z}}_p^n = \mathbf{Z}_p^n + \mathbf{A}^n \odot \mathbf{Z}_p^n, \quad (6)$$

where $\odot$ is an operation for element-wise multiplication.

Given $\tilde{\mathbf{Z}}_p^n$ from each intermediate layer, we ensemble the features from different blocks by taking advantage of the hierarchical architecture [34, 44]. It is required for recognizing heterogeneous types of attributes such as colors or shapes [49]. Especially, we choose low-, middle-, and high-level features from the backbone, denoted as $\{\tilde{\mathbf{Z}}_p^l, \tilde{\mathbf{Z}}_p^m, \tilde{\mathbf{Z}}_p^h\}$, and ensemble those triplets with global average pooling (GAP) followed by concatenation. The attribute expert E_a then generates an attribute embedding with the triplets as

$$\mathbf{p}_a = E_a([\texttt{GAP}(\tilde{\mathbf{Z}}_p^l), \texttt{GAP}(\tilde{\mathbf{Z}}_p^m), \texttt{GAP}(\tilde{\mathbf{Z}}_p^h)]), \quad (7)$$

where E_a consist of a FC layer. Similar to the object expert, we optimize the attribute expert with the cross-entropy loss:

$$\mathcal{L}_{\text{att}} = -\log \frac{\exp\{cos(\mathbf{p}_a, w(a_i))/\tau_a\}}{\sum_{a_k \in \mathcal{A}} \exp\{cos(\mathbf{p}_a, w(a_k))/\tau_a\}}. \quad (8)$$

3.3. Mapping visual-semantic space

The visual compositional embedding $\mathbf{p}_x$ of the input image x is calculated from object and attribute experts, formulated as

$$\mathbf{p}_x = E_c([\mathbf{p}_o, \mathbf{p}_a])). \quad (9)$$

The embedding function E_c includes an FC layer, projecting the visual features into the joint embedding space that aligns visual and semantic representations. Following previous works [43, 37], we estimate semantic label embedding $\mathbf{p}_y$ of each seen composition label $y \in \mathcal{Y}_s$ by projecting the concatenated word vectors into the joint space:

$$\mathbf{s}_y = g([w(o), w(a)]), \quad (10)$$

where $g(\cdot)$ is a label embedding network that consists of 3 FC layers and ReLU activation function. During training, we minimize the cosine distance of visual and semantic embeddings with cross-entropy loss as follows:

$$\mathcal{L}_{\text{comp}} = -\log \frac{\exp\{cos(\mathbf{p}_x, \mathbf{s}_y)/\tau_c\}}{\sum_{y_k \in \mathcal{Y}_s} \exp\{cos(\mathbf{p}_x, \mathbf{s}_{y_k}))/\tau_c\}}, \quad (11)$$

where τ_c is a temperature parameter for the composition loss $\mathcal{L}_{\text{comp}}$. Finally, the total objectives of CoT is then formulated as follows:

$$\mathcal{L}_{\text{total}} = \mathcal{L}_{\text{comp}} + \alpha \mathcal{L}_{\text{att}} + \beta \mathcal{L}_{\text{obj}}, \quad (12)$$

where α and β are balance weights.

During inference, we measure the cosine similarity between a visual embeddings and all label embeddings from $\mathcal{Y}_{\text{te}}$ and regard it as a feasibility score of the image and composition labels [37]. Following [81], we also use the classification scores from object and attribute experts as a form of cosine similarity. Therefore, a final feasibility score of label $y = (a, o)$ is derived by adding the above three scores, formulated as:

$$c(y) = cos(\mathbf{p}_x, \mathbf{s}_y) + cos(\mathbf{p}_o, w(o)) + cos(\mathbf{p}_a, w(a)), \quad (13)$$

where we predict the label with the highest score as the final composition label.
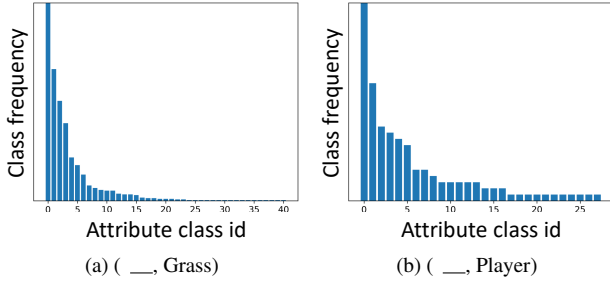
(a) (__ , Grass)   (b) (__ , Player)

Figure 3: Attribute class distributions on VAW-CZSL. Every attributes in each plot are composed into a fixed object; (a) Grass and (b) Player.

3.4. Minority attribute augmentation

With a carefully designed architecture, our CoT can generate distinctive visual features for CZSL. Nevertheless, the imbalanced composition samples in the training dataset restrict the performance since attributes often co-occur with certain objects in the real world [31]. For example in Fig. 3, 'Green Grass' is naturally more common than 'White Grass'. Such long-tailed data makes the deep models be over-confident in the composition with head attributes [82], and thus hurts the generalization on unseen compositions.

To this end, we present a minority attribute augmentation (MAA) for training, which diversifies the minority composition. First, two compositional embeddings from CoT are selected as inputs to the augmentation, where $\mathbf{p}_{x_A}$ and $\mathbf{p}_{x_B}$ share the same object class. Especially, to balance the major and minor attributes, we assign higher sampling weights on minority attributes with the weighted sampler [14]. Formally, let ζ_{o_i} denote the number of attribute samples in the i-th attribute class composed on an object class o. The sampling weight of the attribute-object pair $\kappa(a_i, o)$ is formulated by an inverse attribute class frequency according to:

$$\kappa(a_i, o) = \frac{1/\zeta_{o_i}}{\sum_i 1/\zeta_{o_i}}. \tag{14}$$

Inspired by Mixup [80, 65], we generate a virtual sample $\mathbf{p}_{x_M}$ with alpha compositing and its attribute semantic embedding $w(a_M)$ by linear combination:

$$\mathbf{p}_{x_M} = \lambda \mathbf{p}_{x_A} + (1 - \lambda)\mathbf{p}_{x_B},$$
$$w(a_M) = \lambda w(a_A) + (1 - \lambda)w(a_B). \tag{15}$$

The mixing factor λ is sampled from a uniform distribution.

We notice that there are two significant differences from Mixup: (1) Compared to Mixup sampling arbitrary images, MAA constructs a composition pair fastening an object with the minority aware sampling to address the imbalanced data issue in CZSL. (2) Mixup mixes one-hot vector labels [80, 78] for classification, while MAA generates a

virtual label in word vector space, to jointly regularize visual and linguistic (label) embedding functions against the majority attribute classes with Eq. (12).

3.5. Extension to other backbones

Our idea of CoT is generic and scalable, so we can simply extend to other backbones such as ResNet-18 (R18) [17] by selecting specific layers from the backbone composed of multiple layers or blocks. For a fair comparison to prior arts [42, 54, 24], we study the impact of our contribution on the ResNet backbone based on the convolutional operation. In specific, the object expert generates the object embedding from the last fifth convolution block. The classification token is replaced by a global average pooled feature. Similar to using ViT [11], we concatenate the intermediate layers into a feature vector for the attribute expert. The remained settings such as the architecture of E_{comp} and $g(\cdot)$ are the same as ViT.

4. Experiments

4.1. Experimental setup

Datasets. MIT-States [20] dataset is a common dataset in CZSL that most previous methods adopted, containing 115 states , 245 object, and 1962 compositions. C-GQA [42] and VAW-CZSL [54] are two brand-new and large-scale benchmarks collected from in-the-wild images with more general compositions, such as 'Stained Wall' and 'Hazy Mountain'. Detailed data statistics including long-tailed distribution can be found in Appendix A.

Metrics. We follow common CZSL setting [50], testing performance on both seen and unseen pairs [5]. Under the setting, we report area under the curve (AUC) (%) between seen and unseen accuracies at different bias term in validation and test splits. We also compute the best seen and unseen accuracies in the curve, and calculate the best harmonic mean to measure the trade-off between the two values. Lastly, we follow [42] and report the attribute and object accuracies on unseen labels to measure the discrimination power of each representation.

Baselines. We compare our CoT with 9 recent CZSL approaches: AoP [43], LE+ [40], TMN [50], Symnet [30], CompCos [37], CGE [42], SCEN [28], OADis [54], CAPE [24]. All baselines were built on pretrained ResNet-18 (R18) [17], with pre-trained word embedding such as GloVe [48], FastText [4], and Word2Vec [38]. To show the contribution of our proposed elements, we carry on the most recent methods including CGE and OADis with a transformer-based backbone (ViT-B) [11]. We also clarify that CGE and OADis utilize the knowledge of unseen composition labels at training for building a relation graph and hallucinating virtual samples respectively, while other methods do not assess the unseen composition label sets. The results of other baselines were obtained from

Methods	Backbone	MIT-States					C-GQA					VAW-CZSL				
		V@1	T@1	HM	S	U	V@1	T@1	HM	S	U	V@3	T@3	HM	S	U
With frozen R18																
AoP [43]	R18	2.5	2.0	10.7	16.6	18.4	0.9	0.3	2.9	11.8	3.9	1.4	1.4	9.1	16.4	11.7
LE+ [40]	R18	3.5	2.3	11.5	16.2	21.2	1.2	0.6	5.3	16.1	5.0	1.5	1.6	9.8	16.2	13.2
TMN [50]	R18	3.3	2.6	11.8	22.7	17.1	2.2	1.1	7.7	21.6	6.3	2.2	2.3	11.9	19.9	15.4
Symnet [30]	R18	4.5	3.4	13.8	24.8	20.0	3.3	1.8	9.8	25.2	9.2	2.3	2.3	12.2	19.1	15.8
CompCos [37]	R18	6.9	4.8	16.9	26.9	24.5	3.5	2.6	12.1	28.1	11.8	3.1	3.2	14.2	23.9	18.0
CGE* [42]	R18	7.2	5.3	18.1	28.9	25.0	3.6	2.5	11.9	27.5	11.7	2.7	2.9	13.0	23.4	16.8
SCEN [28]	R18	7.2	5.3	18.4	29.9	25.2	4.0	2.9	12.4	28.9	12.1	-	-	-	-	-
OADis* [54]	R18	<u>7.6</u>	<u>5.9</u>	18.9	**31.1**	25.6	-	-	-	-	-	<u>3.5</u>	<u>3.6</u>	15.2	**24.9**	<u>18.7</u>
CAPE [24]	R18	-	5.8	<u>19.1</u>	30.5	<u>26.2</u>	-	4.2	16.3	32.9	15.6	-	-	-	-	-
CoT	R18	**7.7**	**6.2**	**19.6**	<u>30.8</u>	**26.8**	**4.9**	**4.5**	**16.6**	**33.1**	**16.6**	**3.6**	**3.8**	**15.7**	<u>24.6</u>	**19.1**
With frozen ViT-B																
CGE* [42]	ViT-B	8.7	7.3	21.3	33.5	28.6	4.5	3.8	15.6	31.3	14.4	3.7	3.9	15.7	26.3	19.7
OADis* [54]	ViT-B	<u>9.0</u>	<u>7.5</u>	<u>21.9</u>	<u>34.2</u>	<u>29.3</u>	<u>5.9</u>	4.6	16.2	32.5	15.3	<u>4.1</u>	<u>4.3</u>	16.6	**26.9**	20.8
CoT	ViT-B	**9.2**	**7.8**	**23.2**	**34.8**	**31.5**	**6.7**	**5.1**	**17.5**	**34.0**	**18.8**	**4.4**	**4.7**	**17.7**	**26.9**	**22.2**
With finetuning ViT-B																
CGE* [42]	ViT-B	11.4	9.7	24.8	**39.7**	31.6	7.3	5.4	18.5	38.0	17.1	5.9	6.2	20.1	30.1	25.7
OADis* [54]	ViT-B	<u>11.8</u>	<u>10.1</u>	<u>25.2</u>	39.2	<u>32.1</u>	<u>8.1</u>	<u>7.0</u>	<u>20.1</u>	<u>38.3</u>	<u>19.8</u>	<u>6.2</u>	<u>6.5</u>	<u>20.4</u>	<u>31.3</u>	<u>26.1</u>
CoT	ViT-B	**12.1**	**10.5**	**25.8**	<u>39.5</u>	**33.0**	**8.7**	**7.4**	**22.1**	**39.2**	**22.7**	**6.6**	**7.2**	**21.7**	**32.9**	**28.2**

Table 1: Quantitative comparison with prior arts. Following [42, 54], we measure AUC values on validation (V) and test (T) datasets, at top-1 (@1) on C-GQA and top-3 (@3) on VAW-CZSL, respectively. In addition, we report harmonic mean (HM), seen (S), unseen (US), attribute (A), and object (O) accuracies. ∗ denotes the models accessing unseen composition labels at training. The best result and the second best result are boldfaced and underlined, respectively.

[42, 28, 24, 54] or re-implemented from their official code.

4.2. Implementation details

Models. We use ViT-B [11] and ResNet18 [17] pre-trained on ImageNet [9] as a visual backbone. In ViT-B backbone, Each patch size is 16×16, and the number of patch tokens in each layer is 14×14, having 768 channels per token. The label embedding network g is composed of 3 FC layers, two dropout layers with ReLU activation functions, where hidden dimensions are 900. We use one FC layer for E_o and E_a to produce 300-dimensional prototypical vectors that are matched with GloVe [48] embedding vectors from composition labels. Therefore, both E_c and $g(\cdot)$ produce 300-dimensional embedding vectors, with l_2 normalization. In the attribute expert, we use the outputs of the 3rd, 6th and 9th blocks (denoted z^l, z^m, z^h respectively) for multi-level feature fusion. For ResNet18, we use the 2nd, 3rd and 4th blocks as z^l, z^m, z^h, resulting in a 438-dimensional feature vector.

Training setup. We train CoT with Adam optimizer [26]. The input images are augmented with random crop and horizontal flip, and finally resized into 224×224. In ViT, learning rate is initialized to $1e$-4 for all three datasets, and decayed by a factor of 0.1 for 10 epochs. In R18, the initial learning rate is $5e$-5 with the same decay parameter of the ViT setting. Note that we freeze the GloVe [48] word embedding w for fair comparisons. For all datasets, we use the same temperature parameters [37, 54, 28] of each cross-

Methods	MIT-States		C-GQA		VAW-CZSL	
	Attr.	Obj.	Attr.	Obj.	Attr.	Obj.
CGE [42]	<u>35.7</u>	44.4	<u>17.5</u>	34.6	<u>24.5</u>	51.6
OADis [54]	35.2	<u>45.2</u>	14.7	**42.0**	22.3	<u>53.8</u>
CoT	**37.3**	**46.0**	**19.8**	<u>40.2</u>	**27.3**	**54.2**

Table 2: Comparison of unseen attribute (Attr.) and object (Obj.) occuracies with the latest CZSL methods [42, 54]. All results are reported on fine-tuned ViT backbone.

entropy loss, τ_c, τ_o, and τ_a as 0.05, 0.01 and 0.01 respectively. We use the loss balance weights α and β as (0.5, 0.5) on C-GQA, and (0.4, 0.6) on VAW-CZSL and MIT-States. We note that to prevent overfitting of CoT we apply MAA from 15 and 30 epochs to ViT and R18, respectively.

4.3. Main evaluation

Table 1 compares generalization performance between our methods and the baselines with ResNet18 [17] (R18) and ViT-B [11] backbone setting. To further compare visual discrimination, we also compare unseen attribute and object accuracies of our methods and the latest CZSL methods [42, 54] in Table 2. In the following, we analyze the results from the three datasets.

MIT-States. From Table 1, the CoT achieves the best AUC values (V@1 and H@1) and harmonic mean (HM) with both R18 and ViT backbone. These results sufficiently

CoT	MAA	AUC	HM
		5.81	18.1
	✓	6.05	19.0
✓		6.93	20.8
✓	✓	**7.20**	**21.7**

(a) Component analysis.

Loss component	AUC	HM
$\mathcal{L}_{\text{comp}}$	5.94	18.9
$\mathcal{L}_{\text{comp}}+\mathcal{L}_{\text{obj}}$	6.22	19.6
$\mathcal{L}_{\text{comp}}+\mathcal{L}_{\text{attr}}$	6.91	21.4
$\mathcal{L}_{\text{comp}}+\mathcal{L}_{\text{attr}}+\mathcal{L}_{\text{obj}}$	**7.20**	**21.7**

(b) Impact of loss functions.

Augmentation	AUC	HM
Manifold Mixup [65]	5.93	18.8
CutMix [78]	6.95	20.7
Mixup [80]	7.04	21.0
MAA	**7.20**	**21.7**

(c) Impact of data augmentation.

Guidance	AUC	HM	S	U	A	O
w/o guidance	6.7	20.5	30.7	25.8	22.5	53.4
Attribute guidance	6.9	21.0	31.5	26.4	25.7	53.9
Object guidance	**7.2**	**21.7**	**32.9**	**28.2**	**27.3**	**54.2**

(d) Impact of object guidance.

Ensemble	z_l	z_m	z_h	AUC	HM	S	U	A	O
Low	2	3	4	6.6	20.7	30.3	28.7	<u>25.8</u>	52.3
Mid	5	6	7	<u>6.9</u>	21.2	31.9	**29.7**	25.2	**55.9**
High	9	10	11	6.8	<u>21.4</u>	**33.4**	26.6	24.1	<u>54.5</u>
Mixture	3	6	9	**7.2**	**21.7**	<u>32.9</u>	<u>28.2</u>	**27.3**	54.2

(e) Different configurations of intermediate blocks in attribute experts.

Table 3: Ablation experiments on VAW-CZSL dataset. Note that all results are reported on CoT (ViT-B), with a fine-tuning setting.

demonstrate our experts' applicability on the CNN-based backbone. With a finetuned ViT-B, the CoT obtains the best validation AUC of 12.1% and test AUC of 10.5%, surpassing previous CZSL methods with a large margin. Our method also improves attribute (Attr.) and object (Obj.) accuracies as in Table 2, showing the effectiveness of CoT for visual discrimination.

C-GQA. Similar trends can be observed in the C-GQA dataset. In the frozen R18 setting, the CoT achieves the best test AUC (T@1) of 4.5%, comparable with previous state-of-the-art CAPE. Although the T@1 scroes from CGE and OADis are also increased upon replacing the backbone from R18 to ViT-B, our CoT with ViT-B outperforms OADis with larger margins in all metrics, as compared to the performance with R18. It is noticeable that our proposed augmentation technique contributes the unbiased prediction, improving unseen accuracies into 18.8% with a minority-aware sampling. The performance regarding AUC is improved with end-to-end training with backbone, 2.0% in V@1 and 2.3% in T@1. Of note, OADis and CGE access unseen composition labels at training, so it is unfair to directly compare with other methods including CoT. Nevertheless, more surprisingly, our CoT shows comparable and superior performance to OADis. Finally, in Table 2, our model also improves the attribute accuracy by achieving 19.8%, having comparable 40.2% object accuracy compared to OADis and CGE.

VAW-CZSL. We also achieve SoTA performance on VAW-CZSL, the most challenging benchmark having almost 10K composition labels for evaluation. Even if we do not use additional unseen composition information like OADis, our method achieves the highest T@1 of 7.2% with the best unseen label accuracy of 28.2%. We also obtain both the highest attribute and object score (Table 2), especially with a significant improvement in attribute prediction by 2.8% compared to CGE. It proves that the careful modeling of the visual network in CoT is essential to substantially improve

the generalization capability. In addition, the results suggest that finetuning the visual backbone to suit composition recognition improves the performance in all benchmarks.

4.4. Ablation study

We ablate our CoT and MAA with different design choices on Table 3. We use the VAW-CZSL dataset and fine-tuned ViT-B backbone as our main ablation setting.

Component analysis. We report ablation results of CoT and MAA in Table 3a. In 'without CoT' case, we use CompCos [37] baseline. CoT boosts the AUC and HM significantly about 1.1% and 2.3% compared to the baseline. MAA offers better results to both CoT and baseline, showing scalability to other methods. Notably, employing MAA on CoT gives higher gains of 0.3% AUC and 2.3% HM compared to the baseline, demonstrating that the two components create a synergy effect.

Impact of loss functions. Table 3b shows the impact of each loss function. Compared to the case using $\mathcal{L}_{\text{comp}}$ only, $\mathcal{L}_{\text{obj}}$ and $\mathcal{L}_{\text{attr}}$ bring a gain on both AUC and HM. Using both loses to $\mathcal{L}_{\text{comp}}$ improves AUC and HM significantly by 1.26% and 2.8% respectively, showing the importance of object and attribute losses to learn each expert.

Different data augmentations. In Table 3c, we compare MAA with various data mixing methodologies including Manifold Mixup [65], CutMix [78] and Mixup [80]. To apply Manifold Mixup in CoT, we select 3,6,9 and the last layer as a mixup layer, and mix these intermediate features. MAA achieves the highest score on both AUC and HM, outperforming other augmentation methods including standard Mixup. This demonstrates the effectiveness of MAA which balances the data distribution with a composition pair. Interestingly, we found that Manifold Mixup performs at worst, even degrading pure CoT performance (AUC: 6.93, HM: 20.4) in Table 3a. We speculate that the mixed representation at intermediate layers can lead to significant underfitting of the attention module.
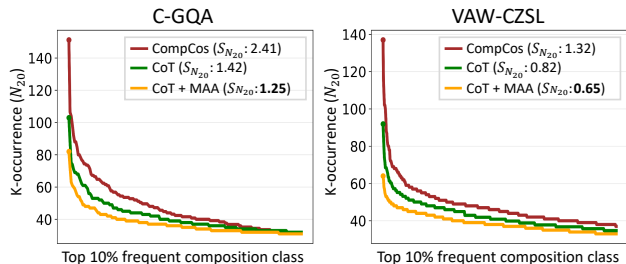
Figure 4: Distribution of k-occurrence counts with k=20 of C-GQA and VAW-CZSL test set. All results are reported with ViT-B backbone. x-axis stands for composition class ids which are ordered by decreasing count numbers. For better visualization, we show the top 10% head composition classes where the hubness is predominant. Circles at start points indicate the most frequent hubs. The result on MIT-States is in the Appendix C.1.
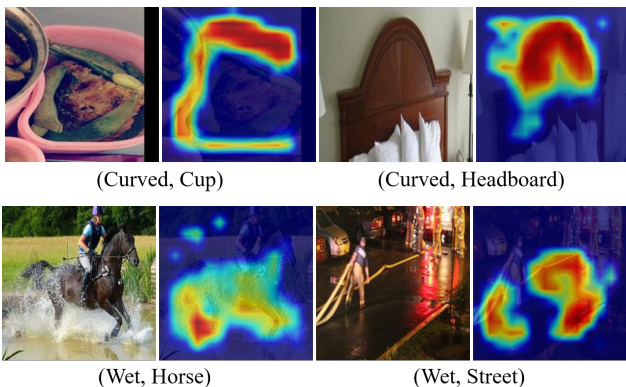

Figure 5: Visualization of object-guided attention on VAW-CZSL dataset. Each row represents the attended regions in image pairs, which are related to different attributes contextualized with a specific object. More results in the Appendix C.5.

Impact of object guidance. As shown in Table 3d, the object guidance significantly boosts the performance. We found that reversing the guidance (attribute guidance) decreases the performance of AUC by 0.3% and HM by 0.7%. The results validate the usage of object guidance for contextualized attribute prediction.

Design choice of feature emsemble. Table 3e shows the ablations with different configurations of intermediate blocks used in the attribute expert. We evaluate four types of block feature ensembles: low, mid, high, and mixture. Among them, the mixture type achieves the best performance on AUC, harmonic mean, and attribute accuracy. We therefore choose this mixture ensemble as a default setting. Another finding is low-level feature is more adequate for attribute and unseen composition recognition, while high-level feature is robust to object and seen composition accuracy.
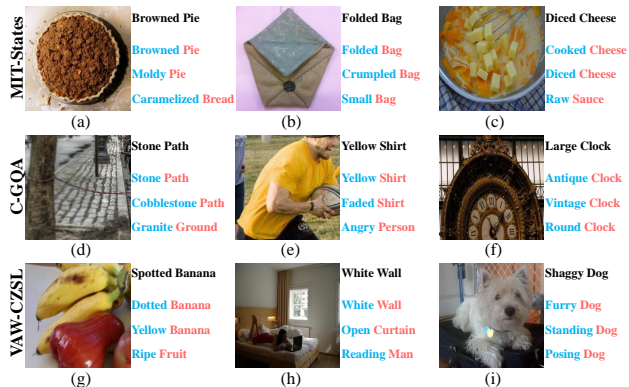

Figure 6: Ground-truth composition labels and top-3 prediction results on MIT-States, C-GQA and VAW-CZSL datasets. More results in the Appendix C.6.

4.5. Discussion

Mitigating hubness problem. We illustrate the hubness effect of a baseline [37] and our method on C-GQA and VAW-CZSL datasets in Fig. 4. Concretely, we count k-occurrences (N_k), the number of times that a sample appears in the k nearest neighbors of other points [51] for all class ids, and calculate the skewness of N_k distribution for hubness measurement. We observe that CoT significantly alleviates the hubness problem of baseline across datasets, enlarging the visual discrimination in the embedding space. MAA further reduces the skewness of the distribution by mitigating biased prediction on head composition classes.

Object-guided attention visualization. Qualitatively, we visualize attention maps from the object-guided attention module in Fig. 5. We observe that the attention module could capture the contextualized meaning of attributes in composition, *e.g.*, wet skin of horse *vs.* puddle in street. It validates that the attention module assists CoT to extract distinctive attribute embedding for composition by localizing specific RoI.

Qualitative results. Fig. 6 illustrates the qualitative results of CoT. Even though some predictions do not correspond to annotated image labels, they explain the composition in another view; *e.g.*, 'Furry Dog' and 'Shaggy Dog' in Fig. 6 (i). Moreover, in-the-wild images usually have multiple objects with their own attributes; *e.g.*, 'White Wall' and 'Reading Man' in Fig. 6 (h). To recognize such compositions in the real world, it is necessary to handle the multi-label nature of composition, while distinguishing each attribute-object interaction [18] in an image. It encourages us to construct a new CZSL benchmark along with a novel evaluation metric handling both multi-label prediction and multiple compositions in the image. We leave it as a future work.

5. Conclusion

In this paper, we propose Composition Transformer (CoT) with simple minority attribute augmentation (MAA), a contextual, discriminative, and unbiased CZSL framework. The proposed object and attribute experts hierarchically utilize the entire powerful visual backbone to generate a composition embedding. The simple but effective MAA balances the long-tail distributed composition labels. Extensive studies with comprehensive analysis demonstrate the effectiveness of each component, and show that CoT surpasses existing methods across several benchmarks.

References

[1] Peter Anderson, Xiaodong He, Chris Buehler, Damien Teney, Mark Johnson, Stephen Gould, and Lei Zhang. Bottom-up and top-down attention for image captioning and visual question answering. In *Proceedings of the IEEE conference on computer vision and pattern recognition*, pages 6077–6086, 2018. 3, 4

[2] Arthur Asuncion and David Newman. Uci machine learning repository, 2007. 2

[3] Yuval Atzmon, Felix Kreuk, Uri Shalit, and Gal Chechik. A causal view of compositional zero-shot recognition. In *NeurIPS*, 2020. 2

[4] Piotr Bojanowski, Edouard Grave, Armand Joulin, and Tomas Mikolov. Enriching word vectors with subword information. *TACL*, 2017. 5

[5] Wei-Lun Chao, Soravit Changpinyo, Boqing Gong, and Fei Sha. An empirical study and analysis of generalized zero-shot learning for object recognition in the wild. In *ECCV*, 2016. 3, 5

[6] Yanbei Chen, Shaogang Gong, and Loris Bazzani. Image search with text feedback by visiolinguistic attention learning. In *Proceedings of the IEEE/CVF Conference on Computer Vision and Pattern Recognition*, pages 3001–3011, 2020. 4

[7] Hsin-Ping Chou, Shih-Chieh Chang, Jia-Yu Pan, Wei Wei, and Da-Cheng Juan. Remix: rebalanced mixup. In *ECCV*, 2020. 2, 3

[8] Yu-Ying Chou, Hsuan-Tien Lin, and Tyng-Luh Liu. Adaptive and generative zero-shot learning. In *International conference on learning representations*, 2020. 3

[9] Jia Deng, Wei Dong, Richard Socher, Li-Jia Li, Kai Li, and Li Fei-Fei. Imagenet: A large-scale hierarchical image database. In *CVPR*, 2009. 6

[10] Georgiana Dinu, Angeliki Lazaridou, and Marco Baroni. Improving zero-shot learning by mitigating the hubness problem. *arXiv preprint arXiv:1412.6568*, 2014. 2, 3, 12

[11] Alexey Dosovitskiy, Lucas Beyer, Alexander Kolesnikov, Dirk Weissenborn, Xiaohua Zhai, Thomas Unterthiner,

Mostafa Dehghani, Matthias Minderer, Georg Heigold, Sylvain Gelly, et al. An image is worth 16x16 words: Transformers for image recognition at scale. In *ICLR*, 2020. 3, 5, 6

[12] Nanyi Fei, Yizhao Gao, Zhiwu Lu, and Tao Xiang. Z-score normalization, hubness, and few-shot learning. In *Proceedings of the IEEE/CVF International Conference on Computer Vision*, pages 142–151, 2021. 2, 3

[13] Chelsea Finn, Pieter Abbeel, and Sergey Levine. Model-agnostic meta-learning for fast adaptation of deep networks. In *ICML*, 2017. 2

[14] Yonatan Geifman and Ran El-Yaniv. Deep active learning over the long tail. *arXiv preprint arXiv:1711.00941*, 2017. 3, 5

[15] Golnaz Ghiasi, Tsung-Yi Lin, and Quoc V Le. Dropblock: A regularization method for convolutional networks. In *NIPS*, 2018. 12

[16] Haibo He and Edwardo A Garcia. Learning from imbalanced data. *IEEE TKDE*, 2009. 3

[17] Kaiming He, Xiangyu Zhang, Shaoqing Ren, and Jian Sun. Deep residual learning for image recognition. In *CVPR*, 2016. 2, 5, 6, 13

[18] Zhi Hou, Xiaojiang Peng, Yu Qiao, and Dacheng Tao. Visual compositional learning for human-object interaction detection. In *ECCV*, 2020. 8

[19] Dat Huynh and Ehsan Elhamifar. Fine-grained generalized zero-shot learning via dense attribute-based attention. In *CVPR*, 2020. 4

[20] Phillip Isola, Joseph J Lim, and Edward H Adelson. Discovering states and transformations in image collections. In *CVPR*, 2015. 5, 12, 13

[21] Mahdi M Kalayeh and Mubarak Shah. On symbiosis of attribute prediction and semantic segmentation. *IEEE TPAMI*, 2019. 3

[22] Shyamgopal Karthik, Massimiliano Mancini, and Zeynep Akata. Revisiting visual product for compositional zero-shot learning. In *NeurIPSW*, 2021. 1

[23] Shyamgopal Karthik, Massimiliano Mancini, and Zeynep Akata. Kg-sp: Knowledge guided simple primitives for open world compositional zero-shot learning. In *CVPR*, 2022. 2, 4, 13

[24] Muhammad Gul Zain Ali Khan, Muhammad Ferjad Naeem, Luc Van Gool, Alain Pagani, Didier Stricker, and Muhammad Zeshan Afzal. Learning attention propagation for compositional zero-shot learning. *arXiv preprint arXiv:2210.11557*, 2022. 5, 6

[25] Hanjae Kim, Sunghun Joung, Ig-Jae Kim, and Kwanghoon Sohn. Prototype-guided saliency feature learning for person search. In *Proceedings of the IEEE/CVF Conference on Computer Vision and Pattern Recognition*, pages 4865–4874, 2021. 4

[26] Diederik P Kingma and Jimmy Ba. Adam: A method for stochastic optimization. In *ICLR*, 2015. 6

[27] Ranjay Krishna, Yuke Zhu, Oliver Groth, Justin Johnson, Kenji Hata, Joshua Kravitz, Stephanie Chen, Yannis Kalantidis, Li-Jia Li, David A Shamma, et al. Visual genome: Connecting language and vision using crowdsourced dense image annotations. *IJCV*, 2017. 2

[28] Xiangyu Li, Xu Yang, Kun Wei, Cheng Deng, and Muli Yang. Siamese contrastive embedding network for compositional zero-shot learning. In *CVPR*, 2022. 2, 5, 6

[29] Yanghao Li, Hanzi Mao, Ross Girshick, and Kaiming He. Exploring plain vision transformer backbones for object detection. In *European Conference on Computer Vision*, pages 280–296. Springer, 2022. 2

[30] Yong-Lu Li, Yue Xu, Xiaohan Mao, and Cewu Lu. Symmetry and group in attribute-object compositions. In *CVPR*, 2020. 2, 5, 6

[31] Kongming Liang, Hong Chang, Bingpeng Ma, Shiguang Shan, and Xilin Chen. Unifying visual attribute learning with object recognition in a multiplicative framework. *IEEE TPAMI*, 2018. 2, 4, 5

[32] Tsung-Yi Lin, Piotr Dollár, Ross Girshick, Kaiming He, Bharath Hariharan, and Serge Belongie. Feature pyramid networks for object detection. In *CVPR*, 2017. 2, 3, 4

[33] Shu Liu, Lu Qi, Haifang Qin, Jianping Shi, and Jiaya Jia. Path aggregation network for instance segmentation. In *Proceedings of the IEEE conference on computer vision and pattern recognition*, pages 8759–8768, 2018. 2

[34] Ze Liu, Yutong Lin, Yue Cao, Han Hu, Yixuan Wei, Zheng Zhang, Stephen Lin, and Baining Guo. Swin transformer: Hierarchical vision transformer using shifted windows. In *ICCV*, 2021. 4

[35] Cewu Lu, Ranjay Krishna, Michael Bernstein, and Li Fei-Fei. Visual relationship detection with language priors. In *ECCV*, 2016. 2

[36] Dhruv Mahajan, Ross Girshick, Vignesh Ramanathan, Kaiming He, Manohar Paluri, Yixuan Li, Ashwin Bharambe, and Laurens Van Der Maaten. Exploring the limits of weakly supervised pretraining. In *ECCV*, 2018. 3

[37] Massimiliano Mancini, Muhammad Ferjad Naeem, Yongqin Xian, and Zeynep Akata. Open world compositional zero-shot learning. In *CVPR*, 2021. 1, 2, 4, 5, 6, 7, 8, 12, 13

[38] Tomas Mikolov, Kai Chen, Greg Corrado, and Jeffrey Dean. Efficient estimation of word representations in vector space. In *ICLR*, 2013. 1, 5

[39] Shaobo Min, Hantao Yao, Hongtao Xie, Chaoqun Wang, Zheng-Jun Zha, and Yongdong Zhang. Domain-aware visual bias eliminating for generalized zero-shot learning. In *CVPR*, pages 12664–12673, 2020. 2

[40] Ishan Misra, Abhinav Gupta, and Martial Hebert. From red wine to red tomato: Composition with context. In *CVPR*, 2017. 1, 2, 4, 5, 6

[41] Rafael Müller, Simon Kornblith, and Geoffrey E Hinton. When does label smoothing help? In *NeurIPS*, 2019. 3

[42] Muhammad Ferjad Naeem, Yongqin Xian, Federico Tombari, and Zeynep Akata. Learning graph embeddings for compositional zero-shot learning. In *CVPR*, 2021. 1, 2, 5, 6, 12, 13, 14

[43] Tushar Nagarajan and Kristen Grauman. Attributes as operators: factorizing unseen attribute-object compositions. In *ECCV*, 2018. 1, 2, 4, 5, 6

[44] Muhammad Muzammal Naseer, Kanchana Ranasinghe, Salman H Khan, Munawar Hayat, Fahad Shahbaz Khan, and Ming-Hsuan Yang. Intriguing properties of vision transformers. In *NeurIPS*, 2021. 3, 4

[45] Zizheng Pan, Bohan Zhuang, Jing Liu, Haoyu He, and Jianfei Cai. Scalable vision transformers with hierarchical pooling. In *Proceedings of the IEEE/cvf international conference on computer vision*, pages 377–386, 2021. 2

[46] Seulki Park, Youngkyu Hong, Byeongho Heo, Sangdoo Yun, and Jin Young Choi. The majority can help the minority: Context-rich minority oversampling for long-tailed classification. In *CVPR*, 2022. 2, 3

[47] Genevieve Patterson and James Hays. Coco attributes: Attributes for people, animals, and objects. In *ECCV*, 2016. 2

[48] Jeffrey Pennington, Richard Socher, and Christopher D Manning. Glove: Global vectors for word representation. In *EMNLP*, 2014. 1, 4, 5, 6

[49] Khoi Pham, Kushal Kafle, Zhe Lin, Zhihong Ding, Scott Cohen, Quan Tran, and Abhinav Shrivastava. Learning to predict visual attributes in the wild. In *CVPR*, 2021. 3, 4

[50] Senthil Purushwalkam, Maximilian Nickel, Abhinav Gupta, and Marc'Aurelio Ranzato. Task-driven modular networks for zero-shot compositional learning. In *ICCV*, 2019. 2, 3, 5, 6

[51] Milos Radovanovic, Alexandros Nanopoulos, and Mirjana Ivanovic. Hubs in space: Popular nearest neighbors in high-dimensional data. *Journal of Machine Learning Research*, 11(sept):2487–2531, 2010. 8, 12

[52] René Ranftl, Alexey Bochkovskiy, and Vladlen Koltun. Vision transformers for dense prediction. In *ICCV*, 2021. 4

[53] Frank Ruis, Gertjan Burghouts, and Doina Bucur. Independent prototype propagation for zero-shot compositionality. In *NeurIPS*, 2021. 2

[54] Nirat Saini, Khoi Pham, and Abhinav Shrivastava. Disentangling visual embeddings for attributes and objects. In *CVPR*, 2022. 1, 2, 5, 6, 12, 13, 14, 16

[55] Dvir Samuel, Yuval Atzmon, and Gal Chechik. From generalized zero-shot learning to long-tail with class descriptors. In *WACV*, 2021. 3

[56] Nikolaos Sarafianos, Xiang Xu, and Ioannis A Kakadiaris. Deep imbalanced attribute classification using visual attention aggregation. In *ECCV*, 2018. 3

[57] Edgar Schonfeld, Sayna Ebrahimi, Samarth Sinha, Trevor Darrell, and Zeynep Akata. Generalized zero-and few-shot learning via aligned variational autoencoders. In *CVPR*, 2019. 2

[58] Li Shen, Zhouchen Lin, and Qingming Huang. Relay backpropagation for effective learning of deep convolutional neural networks. In *ECCV*, 2016. 3

[59] Ying Shu, Yan Yan, Si Chen, Jing-Hao Xue, Chunhua Shen, and Hanzi Wang. Learning spatial-semantic relationship for facial attribute recognition with limited labeled data. In *CVPR*, 2021. 3

[60] Christian Szegedy, Vincent Vanhoucke, Sergey Ioffe, Jon Shlens, and Zbigniew Wojna. Rethinking the inception architecture for computer vision. In *CVPR*, 2016. 2

[61] Chufeng Tang, Lu Sheng, Zhaoxiang Zhang, and Xiaolin Hu. Improving pedestrian attribute recognition with weakly-supervised multi-scale attribute-specific localization. In *ICCV*, 2019. 3

[62] Kaihua Tang, Jianqiang Huang, and Hanwang Zhang. Long-tailed classification by keeping the good and removing the bad momentum causal effect. *Advances in Neural Information Processing Systems*, 33:1513–1524, 2020. 2

[63] Bin Tong, Chao Wang, Martin Klinkigt, Yoshiyuki Kobayashi, and Yuuichi Nonaka. Hierarchical disentanglement of discriminative latent features for zero-shot learning. In *CVPR*, pages 11467–11476, 2019. 2

[64] Grant Van Horn, Oisin Mac Aodha, Yang Song, Yin Cui, Chen Sun, Alex Shepard, Hartwig Adam, Pietro Perona, and Serge Belongie. The inaturalist species classification and detection dataset. In *CVPR*, 2018. 2

[65] Vikas Verma, Alex Lamb, Christopher Beckham, Amir Najafi, Ioannis Mitliagkas, David Lopez-Paz, and Yoshua Bengio. Manifold mixup: Better representations by interpolating hidden states. In *International conference on machine learning*, pages 6438–6447. PMLR, 2019. 5, 7

[66] Byron C Wallace and Issa J Dahabreh. Improving class probability estimates for imbalanced data. *KAIS*, 2014. 3

[67] Jianfeng Wang, Thomas Lukasiewicz, Xiaolin Hu, Jianfei Cai, and Zhenghua Xu. Rsg: A simple but effective module for learning imbalanced datasets. In *Proceedings of the IEEE/CVF Conference on Computer Vision and Pattern Recognition*, pages 3784–3793, 2021. 3

[68] Xin Wang, Fisher Yu, Ruth Wang, Trevor Darrell, and Joseph E Gonzalez. Tafe-net: Task-aware feature embeddings for low shot learning. In *CVPR*, 2019. 2

[69] Yu-Xiong Wang, Ross Girshick, Martial Hebert, and Bharath Hariharan. Low-shot learning from imaginary data. In *Proceedings of the IEEE conference on computer vision and pattern recognition*, pages 7278–7286, 2018. 3

[70] Jun Wei, Qin Wang, Zhen Li, Sheng Wang, S Kevin Zhou, and Shuguang Cui. Shallow feature matters for weakly supervised object localization. In *CVPR*, 2021. 3

[71] Kun Wei, Muli Yang, Hao Wang, Cheng Deng, and Xianglong Liu. Adversarial fine-grained composition learning for unseen attribute-object recognition. In *ICCV*, 2019. 3

[72] Sanghyun Woo, Jongchan Park, Joon-Young Lee, and In So Kweon. Cbam: Convolutional block attention module. In *ECCV*, 2018. 4

[73] Zhe Wu, Li Su, and Qingming Huang. Cascaded partial decoder for fast and accurate salient object detection. In *Proceedings of the IEEE/CVF conference on computer vision and pattern recognition*, pages 3907–3916, 2019. 2

[74] Yongqin Xian, Christoph H Lampert, Bernt Schiele, and Zeynep Akata. Zero-shot learning—a comprehensive evaluation of the good, the bad and the ugly. *IEEE TPAMI*, 2018. 3

[75] Jinheng Xie, Cheng Luo, Xiangping Zhu, Ziqi Jin, Weizeng Lu, and Linlin Shen. Online refinement of low-level feature based activation map for weakly supervised object localization. In *ICCV*, 2021. 3

[76] Ziwei Xu, Guangzhi Wang, Yongkang Wong, and Mohan S Kankanhalli. Relation-aware compositional zero-shot learning for attribute-object pair recognition. *IEEE TMM*, 2021. 2, 3

[77] Muli Yang, Cheng Deng, Junchi Yan, Xianglong Liu, and Dacheng Tao. Learning unseen concepts via hierarchical decomposition and composition. In *CVPR*, 2020. 1

[78] Sangdoo Yun, Dongyoon Han, Seong Joon Oh, Sanghyuk Chun, Junsuk Choe, and Youngjoon Yoo. Cutmix: Regularization strategy to train strong classifiers with localizable features. In *ICCV*, 2019. 3, 5, 7, 12

[79] Matthew D Zeiler and Rob Fergus. Visualizing and understanding convolutional networks. In *ECCV*, 2014. 3

[80] Hongyi Zhang, Moustapha Cisse, Yann N Dauphin, and David Lopez-Paz. mixup: Beyond empirical risk minimization. *arXiv preprint arXiv:1710.09412*, 2017. 2, 3, 5, 7

[81] Tian Zhang, Kongming Liang, Ruoyi Du, Xian Sun, Zhanyu Ma, and Jun Guo. Learning invariant visual representations for compositional zero-shot learning. *arXiv preprint arXiv:2206.00415*, 2022. 1, 2, 4

[82] Zhisheng Zhong, Jiequan Cui, Shu Liu, and Jiaya Jia. Improving calibration for long-tailed recognition. In *CVPR*, 2021. 2, 3, 5

Appendices

A. Data statistics

Table 4 shows detailed data statistics of MIT-States [20], C-GQA [42] and VAW-CZSL [54]. Compared to MIT-States, the latest C-GQA and VAW-CZSL have a large number of attribute, object and composition labels, effective for discussing CZSL problems on realistic scenarios.

A.1. Long-tailed distribution

In Fig. 7, we visualize the distributions of composition class ids in the training set. All datasets, especially for C-GQA and VAW-CZSL having a large number of composition classes, show the long-tailed distribution of compositions. This is a natural effect because we can easily guess that 'black dog' is more frequent than 'blue dog' in the real world. Fig. 8 illustrates the imbalanced attribute composition (*e.g.*, 'white box' are 8 times more frequent than 'pink box'). However, this phenomenon makes it difficult to predict various and novel compositions. Therefore, we proposed minority attribute augmentation (MAA), which remedies a biased prediction caused by the imbalanced data distribution.

B. Implementation details of MAA

We summarize our training procedure of the proposed MAA in 1.**??** An auxiliary image x_B is sampled with a sampling weight κ, which has a different attribute class to a given input x_A. Then, a virtual sample (x_M, y_M) is generated by blending the input with the sampled auxiliary image. We first optimize the object and attribute experts in CoT with the generated virtual samples utilizing object and attribute losses (*i.e.*, $\mathcal{L}_{obj}$ and $\mathcal{L}_{att}$) in the main paper. To align a virtual visual prototype $\mathbf{p}_{vx}$ from x_M with a semantic prototype $\mathbf{p}_{vy} = g([w(o), w(a_M)])$, we simply modify the compositional loss $\mathcal{L}_{comp}$ with the virtual label as follows:

$$\mathcal{L}_{comp} = -\log \frac{\exp\{d(\mathbf{p}_{vx}, \mathbf{p}_{vy})/\tau_c\}}{\sum_{y_k \in \mathcal{Y}_M} \exp\{d(\mathbf{p}_{vx}, \mathbf{p}_{y_k}))/\tau_c\}}, \quad (16)$$

where $\mathcal{Y}_M = \mathcal{Y}_s \cup \{y_M\}$. We empirically find that directly applying the augmentation at the beginning of training leads to under-fitting. To remedy this, the probability of applying MAA in each training iteration is gradually increased as training goes [78, 15]. Specifically, we fix the initial probability as 0.3 until the fifth epoch, while we linearly increase the probability by adding a factor of 0.1 at every fifth epoch.

C. More results

We provide more complementary results to validate CoT on MIT-States, CGQA and VAL-CZSL benchmarks.

Algorithm 1: Minority attribute augmentation

Require: Training dataset $\mathcal{D}_{tr}$.
Initialize: Model parameter θ.

while *Training* **do**
    for $(x_A, a_A, o) \in \mathcal{D}_{tr}$ **do**
        while $a_B \neq a_A$ **do**
            Sample $(x_B, a_B, o) \in \mathcal{D}_{tr}$ with $\kappa(a_B, o)$
        Get $\mathbf{p}_{x_A}$ and $\mathbf{p}_{x_B}$ from CoT
        Sample $\lambda \sim Beta(1, 1)$
        $\mathbf{p}_{x_M} = \lambda \mathbf{p}_{x_A} + (1 - \lambda)\mathbf{p}_{x_B}$
        $w(a_M) = \lambda w(a_A) + (1 - \lambda)w(a_B)$
        $\theta \leftarrow \theta - \nabla \mathcal{L}_{total}(\mathbf{p}_{x_M}, w(a_M), w(o))$

C.1. Hubness effect

We illustrate a distribution of k-occurrences (N_k) [51] to measure a hubness effect of visual features. Note that different from [10], we calculate the nearest neighbors among visual features (queries) to analyze a hubness problem on the **visual domain** in both Fig. 9 and Fig. 4 in the main paper. To be consistent, the proposed CoT and MAA significantly alleviate the hubness problem by enhancing visual discrimination.

C.2. Component analysis

In Table 5, we show the impact of each component (CoT and MAA) for CZSL performance on MIT-States and C-GQA datasets. The ablation results together with Table 3a in the main paper demonstrate that both CoT and MAA consistently give improvements in AUC and HM.

C.3. Other sampling weights

In Table 6, we conduct an ablation study for three different sampling weights leveraging an inverse attribute frequency $1/(\zeta_{o_i})$. Notably, the frequency of $1/(\zeta_{o_i})^2$ yields worse performance. It is under-fitting because sampling few tail class samples with too high probabilities prevents learning with other majority classes. Sampling with square-root frequency, $1/(\zeta_{o_i})^{0.5}$, improves the performance on AUC and HM, but slightly below the result with $1/(\zeta_{o_i})$. We will include the above discussion in the paper.

C.4. Open World setting

To further analyze the generalization performance, we evaluate our CoT on Open World setting [37] in Table 7. Following [37], we compute the best seen (S), unseen (U) accuracies, area under curve (AUC) and the best harmonic mean (HM). Our method also performs well in Open world setting, outperforming previous state-of-the-art methods in all metrics except the best seen accuracy. This result demonstrates that enlarging visual discrimination with

Dataset	#Attribute / #Object	Train		Validation		Test	
		$\mathcal{Y}_s$	#img	$\mathcal{Y}_s$ / $\mathcal{Y}_u$	#img	$\mathcal{Y}_s$ / $\mathcal{Y}_u$	#img
MIT-States[20]	115 / 245	1262	30338	300 / 300	10420	400 / 400	12995
C-GQA[42]	453 / 870	6963	26920	1173 / 1368	7280	1022 / 1047	5098
VAW-CZSL[54]	440 / 541	11175	72203	2121 / 2322	9524	2449 / 2470	10856

Table 4: The statistics of three benchmarks: MIT-States[20], C-GQA[42] and VAW-CZSL[54].

(a) MIT-States   (b) C-GQA   (c) VAW-CZSL
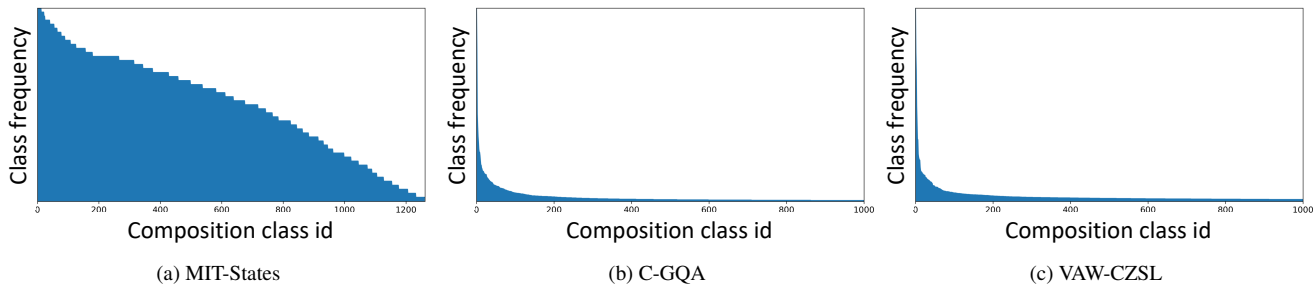
Figure 7: Composition class distribution on three datasets. x-axis (composition class id) is ordered by decreasing composition frequency. For better visualization, we plot the top 1000 frequent composition classes on (b) and (c).
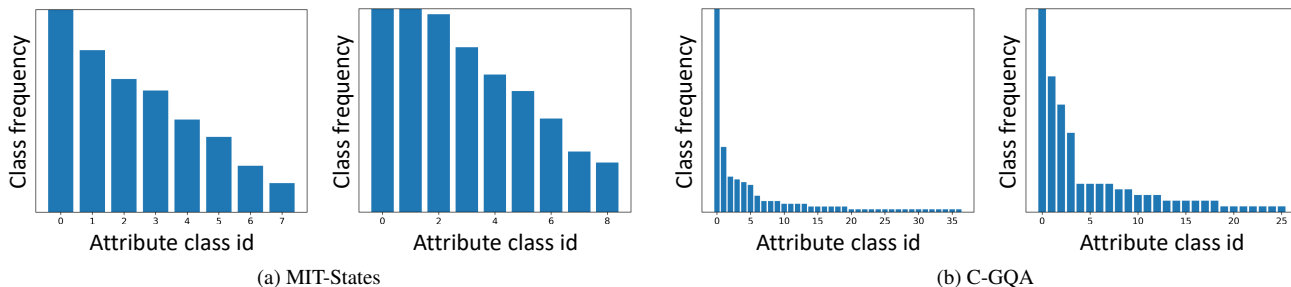

(a) MIT-States   (b) C-GQA

Figure 8: Attribute class distributions on MIT-States and C-GQA. Every attributes in each plot are composed into a fixed object; 'Silk', 'Bucket', 'Street', and 'Box'. (from left to right).

CoT	MAA	AUC	HM
		8.89	22.9
	✓	9.08	23.5
✓		10.26	25.2
✓	✓	**10.54**	**25.8**

(a) MIT-States

CoT	MAA	AUC	HM
		5.25	17.6
	✓	5.58	20.3
✓		7.07	21.2
✓	✓	**7.42**	**22.1**

(b) C-GQA

Table 5: Component analysis on MIT-States and C-GQA dataset.

Methods	S	U	AUC	HM
CompCos [37]	25.4	<u>10.0</u>	8.9	1.6
CGE [42]	32.4	5.1	6.0	1.0
KG-SP [23]	28.4	7.5	7.4	1.3
Ours (CoT)	<u>28.8</u>	**11.3**	**9.5**	**1.8**

Table 7: Open-world CZSL results on MIT-States. All methods use Resnet18 [17] backbone with a fine-tunning setup.

Frequency type	AUC	HM
$1/(\zeta_{o_i})^{0.5}$	7.19	21.5
$1/(\zeta_{o_i})^2$	7.07	21.2
$1/(\zeta_{o_i})$ [default setting in paper]	**7.20**	**21.7**

Table 6: Ablation study for different frequency types of MAA on VAW-CZSL.

C.5. Object-guided attention maps

We illustrate the object-guided attention maps in Fig. 10 with VAW-CZSL, and Fig. 11 with C-GQA. For visualization, we merge three attention maps from low, middle and high blocks through multiplication. The results demonstrate that the attention module could capture the contextualized regions for each attribute, enhancing the visual discrimination of attribute prototypes and its composition.
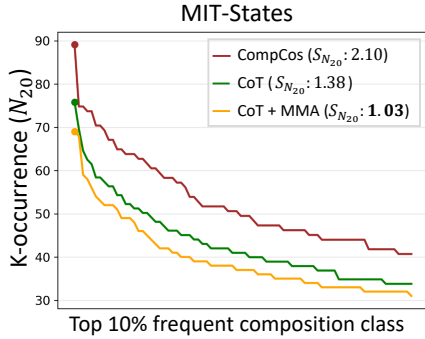
context modeling could also mitigate unfeasible compositions [37] from a large output space of Open World scenario.

Figure 9: Distribution of k-occurence counts (N_k) of MIT-States test set. We use the same setting with Fig. 4 in main paper.

Methods	# Parameters (M)	GFLOPs
OADis[54]	2.25	11.2
CoT	3.34	11.8

Table 8: Comparison of computational complexity between OADis [54] and CoT. Note that backbone (ViT-B) is excluded to count the parameters.

C.6. Top-3 prediction results

We visualize top-3 prediction results in Fig. 12 with VAW-CZSL, and Fig. 13 with C-GQA. CoT clearly outperforms the baseline [54] to retrieve the relevant composition labels. As discussed in Sec. 4.4 of the main paper, the qualitative results show the limitation of existing CZSL datasets [42, 54] including multi-label composition and multiple attribute-object interaction.

D. Computational Analysis

In Table 8, we compare computational complexity with the previous state-of-the-art OADis [54] by reporting the number of parameters and GFLOPs. Although CoT has more parameters induced from the ensemble of block features, it has almost the same model complexity in terms of GFLOPs, thanks to the parameter-efficient convolution based attention module.
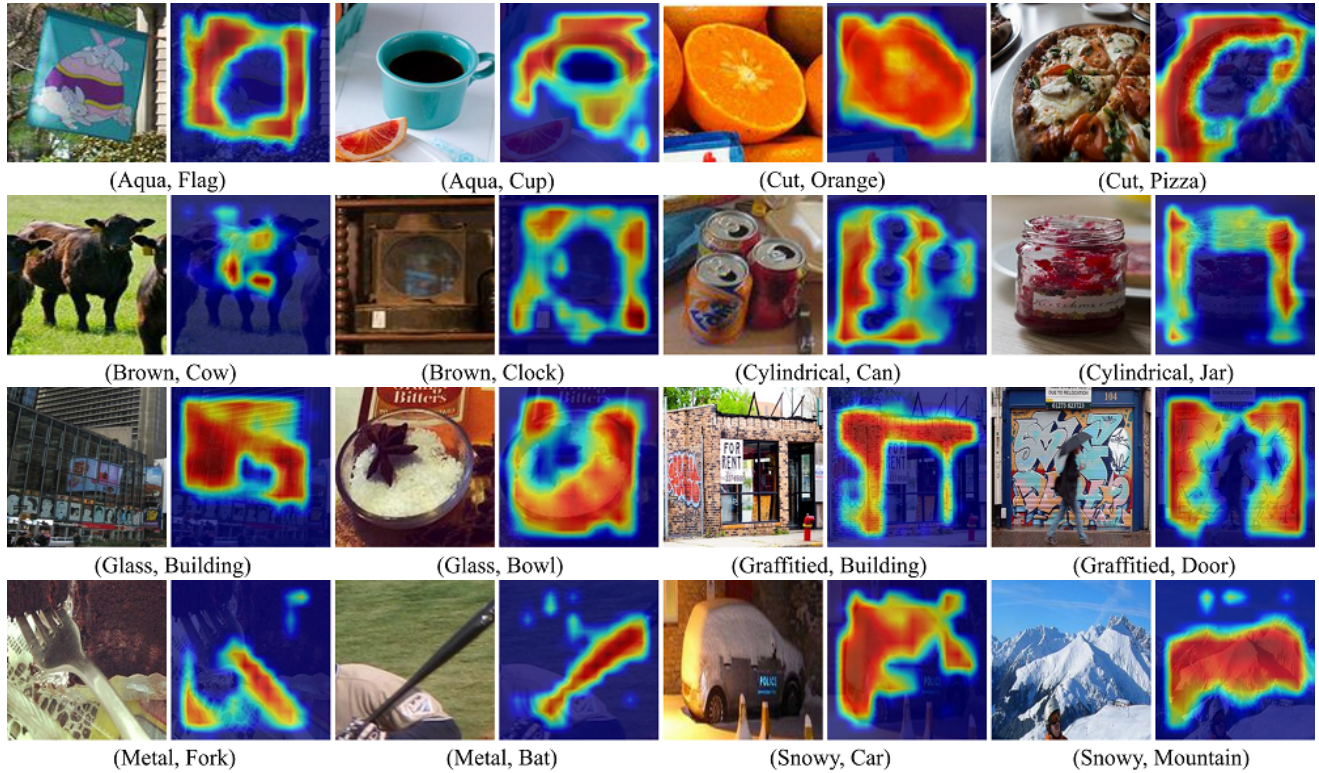
Figure 10: Visualization of object-guided attention maps obtained on **VAW-CZSL**. The input image and attended region by its specific attribute are paired with (attribute, object) labels. (Attention weights: High to Low).
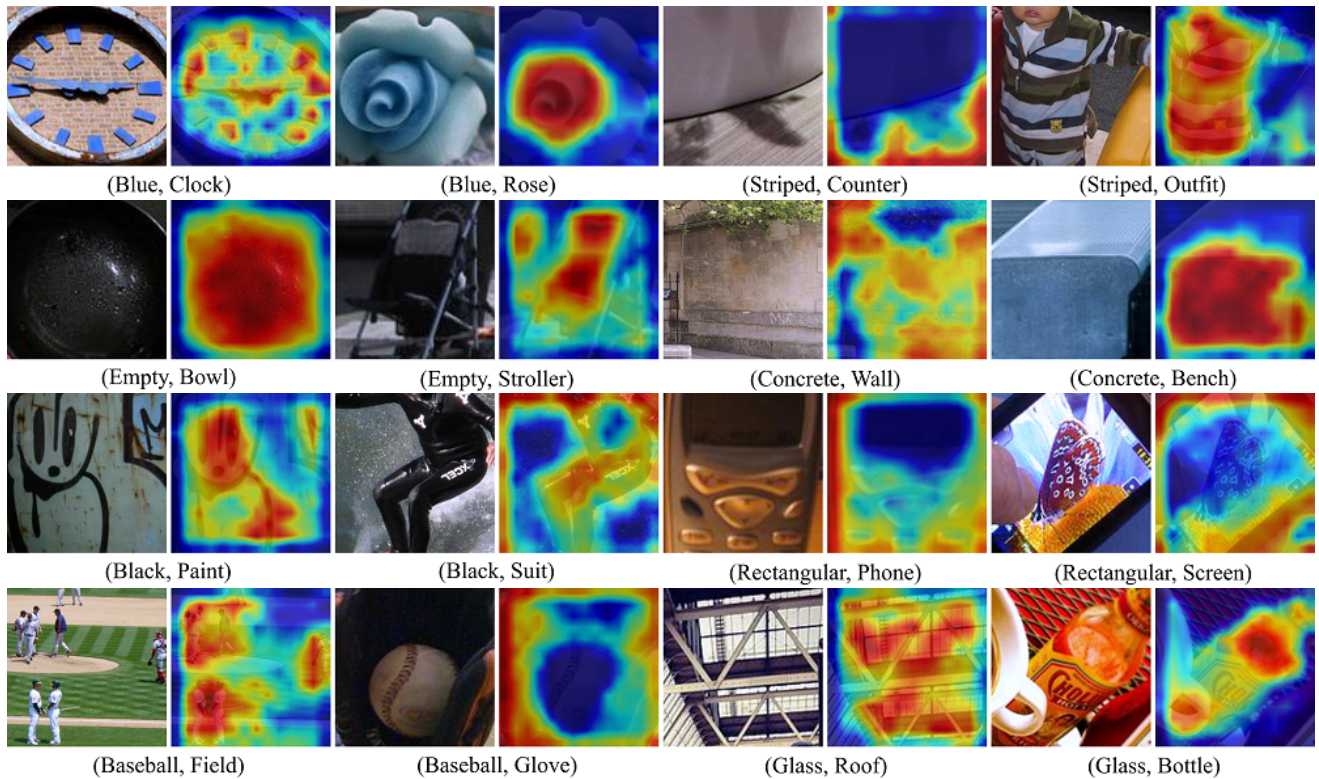

Figure 11: Visualization of object-guided attention maps on **C-GQA**. The input image and attended region by its specific attribute are paired with (attribute, object) labels. (Attention weights: High to Low).
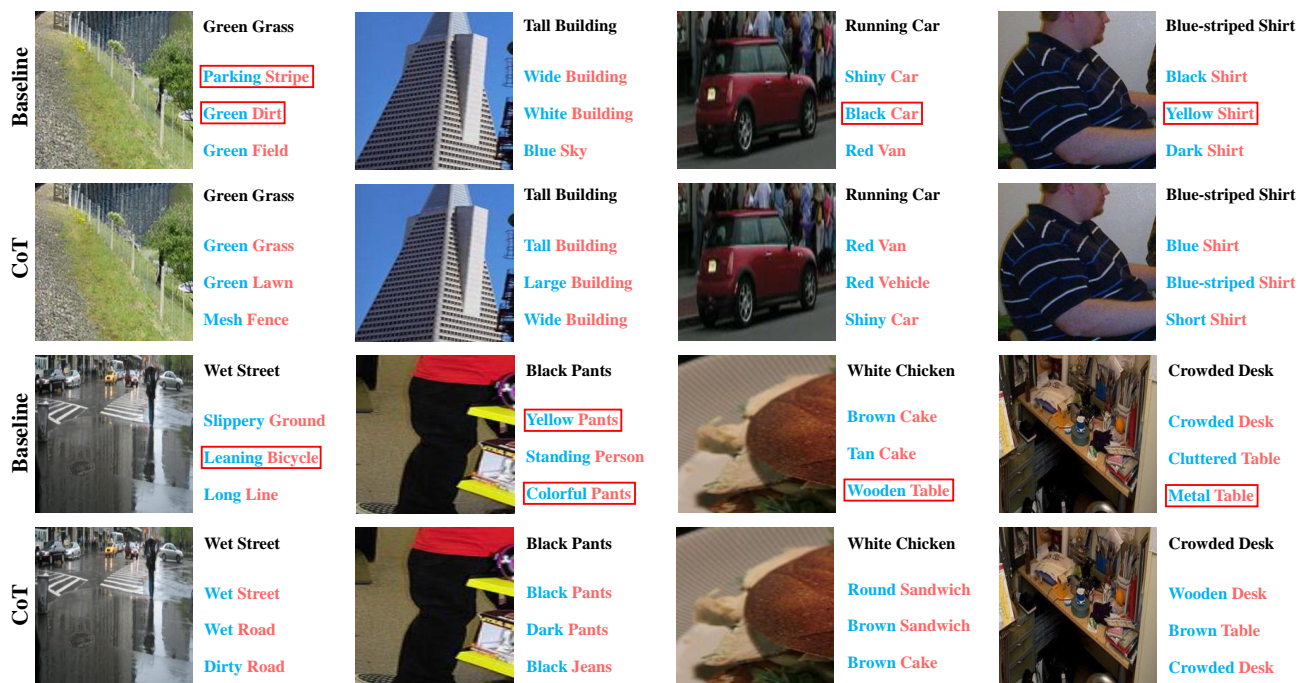
Figure 12: Ground-truth and top-3 prediction results on **VAW-CZSL**. We compare CoT with baseline (OADis) [54]. Red box denotes the false positive, having irrelevant or opposite compared to ground truth.
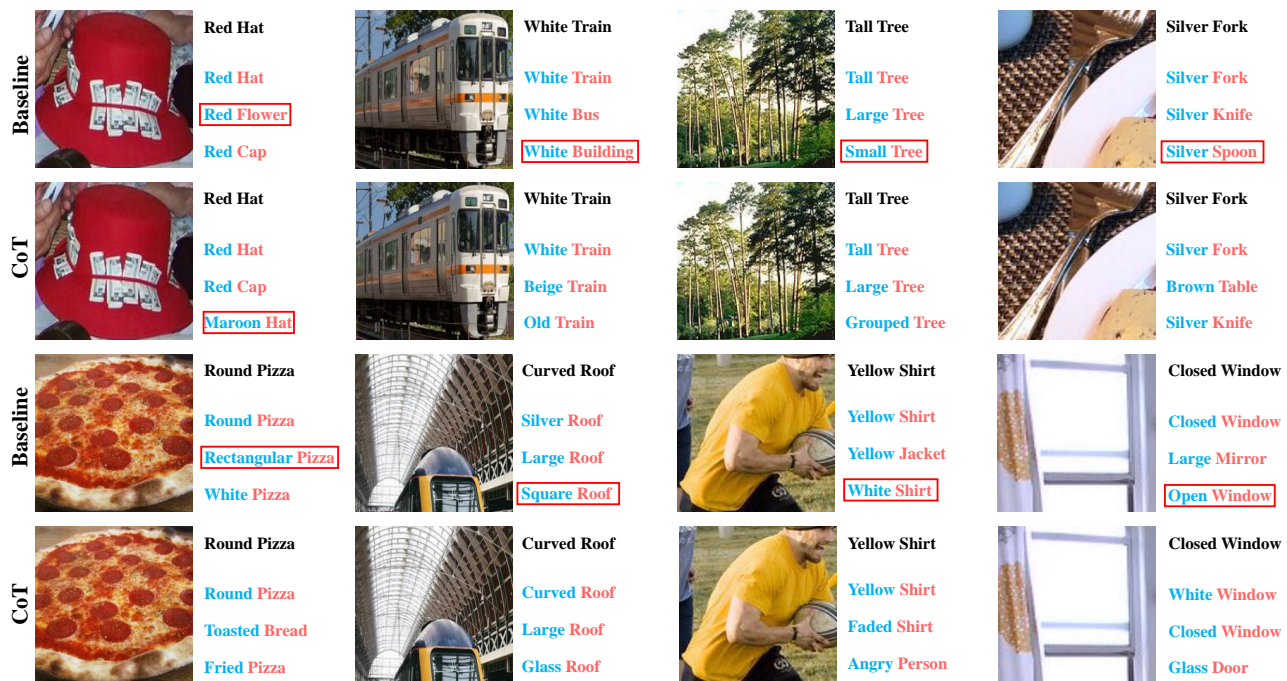

Figure 13: Ground-truth and top-3 prediction results on **C-GQA**. We compare CoT with baseline (OADis) [54]. Red box denotes the false positive, having irrelevant or opposite compared to ground truth.